J Mater Sci: Mater Electron **(2025) 36:1241**

Optical, non-linear optical and electronic properties of 1,3,4-oxadiazole derivative: a combined experimental and theoretical study

Emine Babur ŞAŞ[1,*]

[1] *Department of Electronics and Automation, Vocational School of Technical Sciences, Kirsehir Ahi Evran University, 40100 Kırşehir, Turkey*

Received: 3 February 2025
Accepted: 14 June 2025
Published online: 15 July 2025

ABSTRACT

We investigated the electronic and optical properties of an organic material, 2-(4-bromophenyl)-5-phenyl-1,3,4-oxadiazole (BP-OXA), combining experimental measurements and theoretical calculations. FT-IR and FT-Raman spectra were recorded in the solid phase. The NMR chemical shifts (^{1}H and ^{13}C) were recorded in chloroform solution. The 1H and 13C NMR spectra were computed by using the gauge-invariant atomic orbital (GIAO) method, showing good agreement with the experimental ones. PL studies were utilized to investigate the light-emitting properties of BP-OXA. UV–Vis spectra were recorded in dichloromethane (DCM) at different concentrations, showing strong absorption peaks in the near-UV region (200–400 nm). In the study, we calculated the HOMO–LUMO energy gaps, UV spectra, and optical parameters of the molecule using B3LYP and CAM-B3LYP functional methods and evaluated their compatibility with experimental data. The experimental optical band gap (E_g) of the molecule of approximately 3.84 eV indicates that it has semiconductor properties. Additionally, refractive index values (1.70–2.58) and optical conductivity parameters indicate that BP-OXA is well-suited for optoelectronic applications. The material exhibits robust optical behavior, supported by high dipole moments and significant hyperpolarizability values (5503.52×10^{-33} esu), suggesting potential for advanced photonic technologies. These results highlight BP-OXA as a promising candidate for applications in optoelectronic devices and nonlinear optics.

1 Introduction

Oxadiazole compounds have gained an important place among organic materials in recent years as a versatile field of study with their biological activities, synthesis methods, and semiconductor properties. There are four isomers of the five-membered heterocyclic structure, 1,3,4, 1,2,5, and 1,2,4 1,2,3, according to the nitrogen configuration. The most biologically active of these isomers are 1,3,4-oxadiazole derivatives, and these compounds are also used to prepare donor–acceptor molecules containing π-electron-rich

Address correspondence to E-mail: baburemine@gmail.com

https://doi.org/10.1007/s10854-025-15214-y

aromatic rings. It has been observed that 1,3,4 oxadiazole acts as an electron acceptor when combined with pyrene, increasing charge transfer [1]. Examination of some bis-1,3,4-oxadiazole derivatives with D–π–A (donor–π–acceptor) structure showed that these molecules have high hyperpolarizability values and are promising candidates for NLO applications [2, 3]. In another study, four new 1,3,4-oxadiazole derivative chromophores (TM1–TM4) were developed and the interactions between donor and acceptor groups and intramolecular charge transfer of these compounds were revealed [4].

Due to the high electron affinity of 1,3,4-oxadiazole ring combined with various substituents, it is an important carrier structure investigated for optoelectronic devices such as OLEDs, organic photovoltaics (OPV) and organic solar cells (OSC) [5–9]. For example, Zhao et al. in their study of optical and electrical properties of 1,3,4-oxadiazole derivatives, showed that these compounds provided significant improvements in photovoltaic efficiency [10]. Similarly, Liu et al., by using oxadiazole derivatives in OLEDs, increased the light efficiency [11]. 2-(4-Biphenyl)-5-(4-tert-butylphenyl)-1,3,4-oxadiazole (PBD) showed an electron affinity of 2.16 eV and was first used as an electron carrier material in a double-layer OLED [12]. The compounds formed also affect their physical and chemical properties. In the search for efficient materials for the production of OLEDs, it was found that 2,5-Diaryl-1,3,4-oxadiazoles exhibited suitable properties to be good electron carriers [13]. At the same time, oxadiazole derivatives were found to have thermal and chemical stability and photoluminescence quantum yield [14–19]. Dong et al. investigated the UV–Vis spectra of stilbene-based 1,3,4-oxadiazole derivatives, Nayak et al. investigated the 1,3,4-oxadiazole derivatives containing isobenzofuran group, and Sas et al. investigated the 1,3,4-oxadiazole derivatives containing naphthyl group, and showed that these materials have potential applications in optics [20–22]. Developing high-efficiency fluorescent emitting material is an important issue for high-performance OLED devices [23]. In recent years, OLED fluorescent materials incorporating AD and DAD (donor–acceptor) units have been frequently investigated [24–27]. In addition, a new 1,3,4-oxadiazole derivative, BPOXD-B8, was synthesized and the emission properties of this compound in different solvents were investigated. The organogel formation ability and self-assembly properties of BPOXD-B8 in solvents such as methanol were investigated by SEM, XRD, temperature-dependent FT-IR and UV–Vis spectroscopy [28].

These studies examine the optical properties of 1,3,4-oxadiazole derivatives in detail and show how promising these compounds are in areas such as optoelectronic devices, photovoltaic applications, and biosensors. In order to thoroughly investigate the electronic and optical characteristics of the organic material 2-(4-Bromophenyl)-5-phenyl-1,3,4-oxadiazole (BP-OXA), a derivative of 1,3,4-oxadiazole with a wide range of applications, we employed spectroscopic techniques including FT-IR and FT-Raman, ^{1}H and ^{13}C NMR, PL, and UV–Vis. Using the DFT/B3LYP 6-311G(d,p) approach, we computed the molecule's theoretical data and contrasted it with the experimental data. Based on the molecule's optical and non-linear optical characteristics, we assessed its suitability for use in the optoelectronics industry.

2 Experimental and computational details

We purchased the oxadiazole derivative BP-OXA and the solvent of this molecule DCM from Sigma-Aldrich. FT-IR and FT-Raman spectra of the solid form BP-OXA molecule were recorded using a Thermo Scientific Nicolet 6700 FT-IR/NXR FT-Raman spectrometer at room temperature. Data from both spectra were taken in the range of 4000–400 cm^{-1}. NMR experiments were performed on an Agilent Premium Compact 600 MHz (14.1 Tesla) spectrometer at 300 K. Chemical shifts are reported in ppm for ^{1}H and ^{13}C NMR spectra in chloroform compared to tetramethylsilane (TMS). The PL spectra of the investigated material were recorded at room temperature using a fluorescence spectrophotometer (DONGWOO Maplee II) with PMT (800), Lazer He Cd Detector in the excitation wavelength range of 325 nm, spectral range of 330–960 nm. We prepared the BP-OXA molecule in three different concentrations DCM solvent. We then recorded these concentrations in a UV spectrophotometer (Genesys 10S UV–Vis Spectrophotometer, Thermo Scientific) in the range of 200–1100 nm.

We calculated the geometric structure of the BP-OXA molecule by the DFT/B3LYP/6–311G(d, p) method [29, 30]. After determining the minimum energy structure of the molecule, we used the same method for vibrational spectra. We used the scale factor (0.967) to fit the theoretical vibrational spectra with the experimental spectra [31]. ^{1}H and ^{13}C NMR

chemical shift values of the title molecule were computed in chloroform solvent using B3LYP/6-311G(d,p) basis set by the GIAO method [32]. In order to theoretically investigate the optical parameters and compare them with the experimental data, we obtained the absorbance spectra of the molecule by using the TD-DFT method in two different functionals (B3LYP and CAM-B3LYP) [33, 34]. We obtained the necessary calculations for the molecule from the GAUSSIAN09 package program [35]. In order to examine the HOMO–LUMO energies in detail, we drew the DOS spectrum using the GaussSum 2.2 program [36].

3 Results and discussion

3.1 Molecular structure and vibrational spectral analysis

The BP-OXA molecule, which is a 1,3,4 oxadiazole derivative, consists of bromine atom, phenyl and oxadiazole ring. In order to determine the geometric structure of the molecule, the phenyl rings attached to the oxadiazole rings were rotated around the carbon bonds and the minimum energy state was determined. According to the optimized structure, the minimum energy of the molecule is − 3297.94251432 Hartree and the molecule is planar. Theoretical IR and Raman spectra of BP-OXA molecule were calculated from the optimized structure using 6–311 G(d,p) basis set and are given together with experimental spectra in Fig. 1. C–H stretching vibrations, which are one of the important vibrations in the molecule, generally occur in the range of 3000–3100 cm^{-1} in aromatic rings [37]. In this study, C–H stretching vibrations were calculated in the region between 3064 and 3105 cm^{-1} and this band was named as pure band. These vibration bands were observed at 3058 and 3081 cm^{-1} in FT–IR and at 2987 and 3064 cm^{-1} in FT-Raman. In aromatic rings, C–N and C=N stretching vibrations are generally observed in the range of 1382–1266 cm^{-1} [38]. Similarly, Varsanyi showed C–C and C=C stretching vibrations in the range of 1280–1625 cm^{-1} [39]. These bands are observed mixed in the spectrum. The sharpest peak (1471 cm^{-1}) seen in FT-IR and FT-Raman was assigned as the stretching vibration of C=N and C–C.

C–Br vibrations are not pure vibrations, they are bands mixed with other vibrations of the molecule. Varsanyi gave C–Br vibrations in the long wavelength region (200–480 cm^{-1}) [39]. In our previous study, C–Br vibration band was calculated at 292 cm^{-1} and observed at 308 cm^{-1} in FT-Raman [40]. Sas et al. observed this vibration band at 358 cm^{-1} in FT-Raman and theoretically calculated 396 and 233 cm^{-1} [41]. In this study, we calculated C–Br vibration band at 454 cm^{-1} and observed at 460 cm^{-1} in FT-IR.

3.2 NMR analysis

NMR spectroscopy is one of the most important techniques for structural analysis of organic compounds [42]. To obtain more information about the structural properties of the BP-OXA molecule, ^{1}H and ^{13}C NMR analysis were studied experimentally and theoretically. Experimental NMR spectra and theoretical NMR data of the title molecule are given in Fig. 2a–c, respectively. The chemical shifts of aromatic protons of organic molecules are usually observed in the range of 8.00–7.00 ppm, and the chemical shifts of aromatic carbons are usually observed in the region of 100–150 ppm [43, 44]. Due to the electronic environment of the proton, these chemical shifts can change towards a high or low frequency [45, 46]. We calculated the proton chemical shifts in phenyl rings in the range of 7.63–8.66 ppm. It was observed that the chemical shifts of protons close to the oxadiazole ring shifted to a higher frequency due to the electronic environment. The chemical shift values of these protons in the chloroform solvent are in the range of 7.24–8.24. These values show the agreement of the theoretical and experimental studies. We calculated the chemical shift values of the aromatic carbon atoms of the BP-OXA molecule in the range of 127.4–149.5 ppm and measured experimentally in the range of 122.8–132.5 ppm. The chemical shift values of the two carbon atoms in the oxadiazole ring were calculated as 168.6 and 169.8 ppm, while they were measured experimentally as 163.8 and 164.7 ppm. The proton chemical shift values of the phenyl and oxadiazole rings are in good agreement with the experimental data.

3.3 Photoluminescence (PL) spectroscopy

When a physical system is excited by visible and ultraviolet light, it emits optical radiation known as photoluminescence [47]. A non-contact method called photoluminescence (PL) spectroscopy uses optical excitation to induce spontaneous light emission from a substance. It is frequently used to

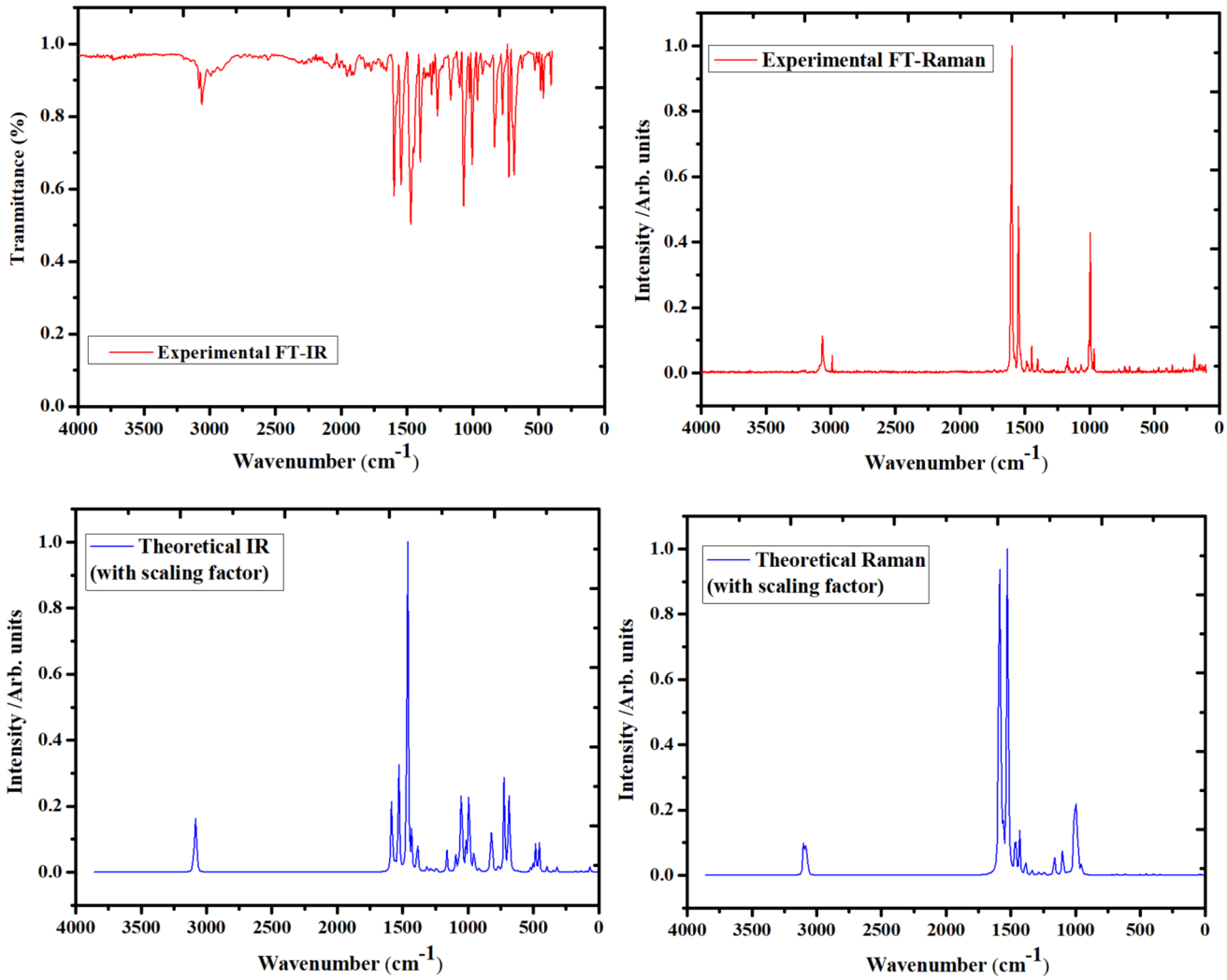

Fig. 1 The experimental and calculated (with the scale factor) FT-IR and FT-Raman spectra of the BP-OXA

explain the material's chemical and physical characteristics [48–50]. The difference in energy levels between the two electronic states is correlated with the photon energies released. An optical spectrometer determines the intensity of these photons in relation to their wavelength [51, 52]. The emission characteristics of the BP-OXA molecule were investigated using PL measurements. Figure 3 shows the PL spectra obtained in the 330–960 nm region. The photoemission transition band is visible at 733 nm (red). The interaction between the activator atoms is known to be the cause of the red shift in the emission bands [53, 54]. Concentration quenching is a phenomena that can happen when the luminescence centers are sufficiently close to one another to cause an interaction [53, 54]. The excitation wavelength (325 nm) is substantially shorter than the main emission beam's wavelength. Its wavelengths are greater than the excitation peaks because it takes more energy for a molecule to move from a lower state to a higher state. The characteristics of fluorescent molecules are determined by the magnitude of the Stokes shift [52]. The primary Stokes shift in this instance is roughly 408 nm. Practically speaking, a big Stokes shift is helpful since it can lessen the "self-quenching" brought on by molecules' self-absorption [55]. Alongside this peak, another peak was seen at 375 nm, which is close to the ultraviolet. Peaks in the near-UV spectrum could be associated with the molecule's functional groups. These results

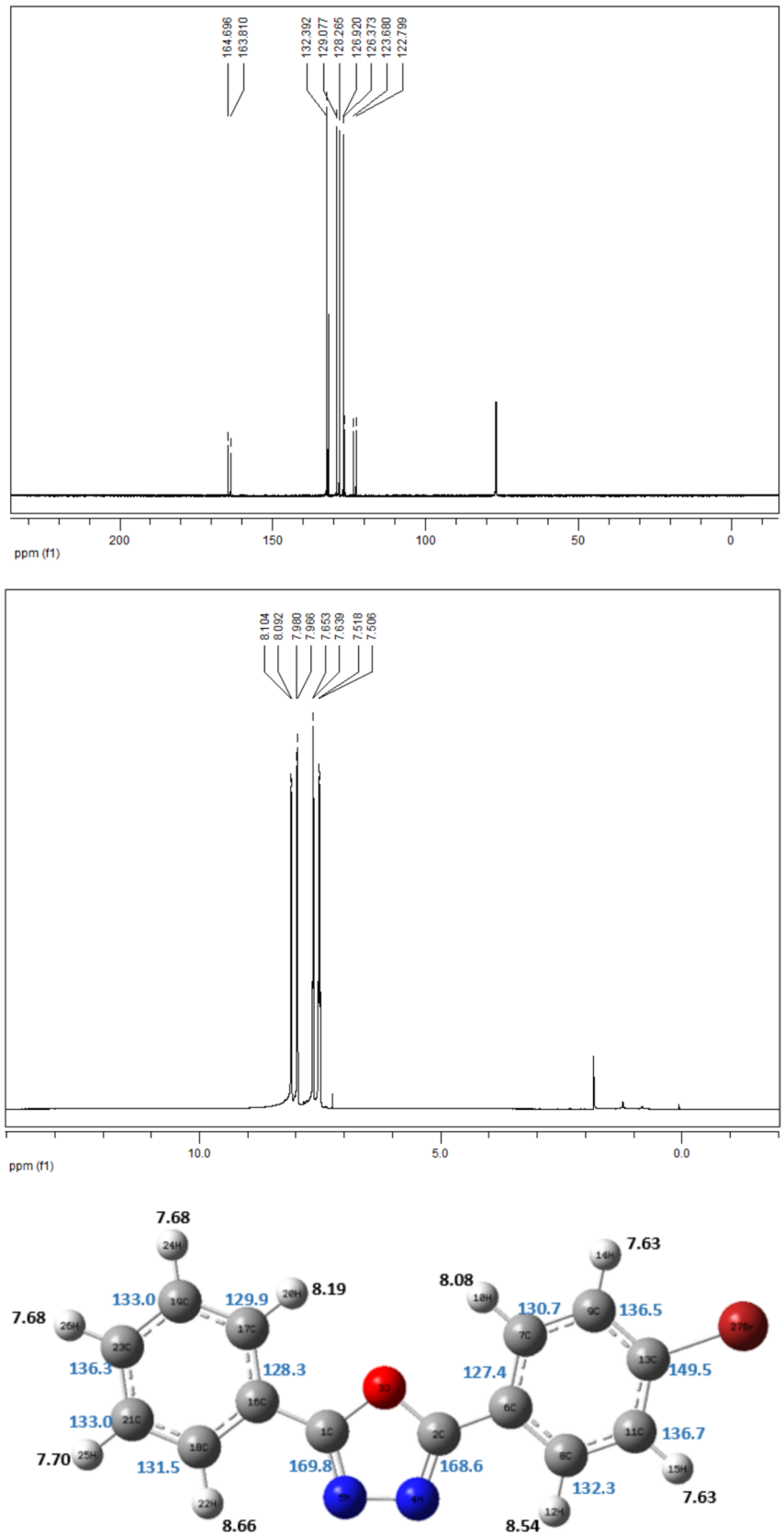

Fig. 2 ^{1}H and ^{13}C NMR spectra of the BP-OXA in chloroform solution

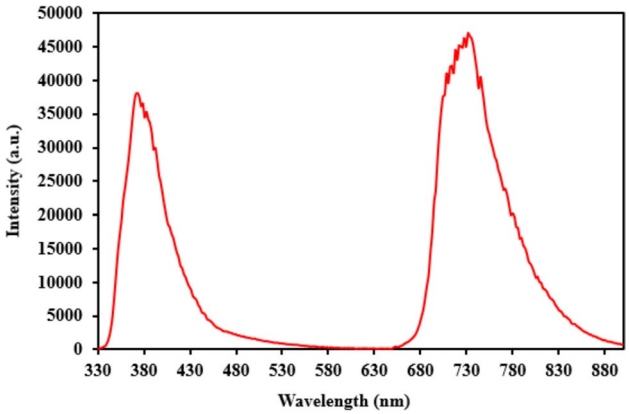

Fig. 3 Photoluminescence spectra for BP-OXA

suggest that the BP-OXA material is suitable for photoluminescence devices.

3.4 UV spectra and optical parameters

We compared the UV spectra measured in DCM solvent and calculated by the TD-DFT method. We gave the UV spectrum calculated in the B3LYP and CAM-B3LYP functionals in the molar absorptivity and wavelength graph (Fig. 4a) and the spectrum measured at different concentrations in the absorbance and wavelength graph (Fig. 4b). We found that the absorbance peaks of BP-OXA recorded at concentrations of 0.189, 0.126, 0.095, and 0.038 mM decreased with decreasing concentration. We can say this by looking at the observed curve of the peaks. From this spectrum, we can say that a maximum peak at 290, a small peak at 234 nm, and a shoulder at 317 nm are observed. The recorded spectral values indicate that the BP-OXA molecule is active in the near UV region (200–400 nm). This figure shows us two important results. First, absorbance and molar absorptivity spectra differ when different methods such as theoretical and experimental methods are used. Second, absorbance and molar absorptivity spectra, which differ in each method, show a slight change at different concentrations. The positions of the maximum peaks are different for the theoretical CAM-B3LYP and B3LYP functionals. The experimental results are consistent for both functionals.

The absorbance band edge ($E_{\text{Abs-be}}$), one of the important optical parameters of the molecules, is obtained from the $dT/d\lambda$ and wavelength graph. $E_{\text{Abs-be}}$ values for four different concentrations were

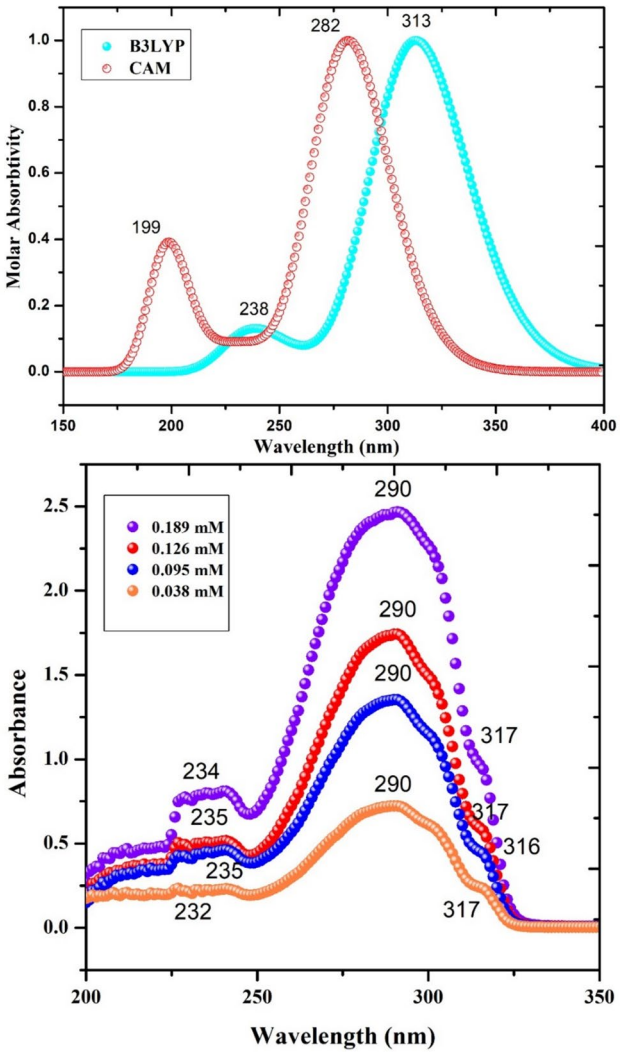

Fig. 4 **a** The theoretical molar absorptivity and wavelength graph and **b** the spectrum measured at different concentrations in the absorbance and wavelength graph of the BP-OXA

obtained as 3.855, 3.853, 3.856, and 3.856 (for concentrations 0.189, 0.038, 0.095, and 0.126 mM), respectively (Fig. 5a, b). The curves show how the optical activity of the molecule is affected by concentration. Spectra recorded at different concentrations reflect the sharpness of the absorption band and energy transitions. According to experimental measurements, this value remained constant despite the concentration change. This shows that the optical constants of BP-OXA in solution are stable and the molecule can exhibit reliable performance in optoelectronic applications. In addition, we calculated this value theoretically with the CAM-B3LYP and B3LYP functionals, and we gave Table 1 together with the experimentally obtained

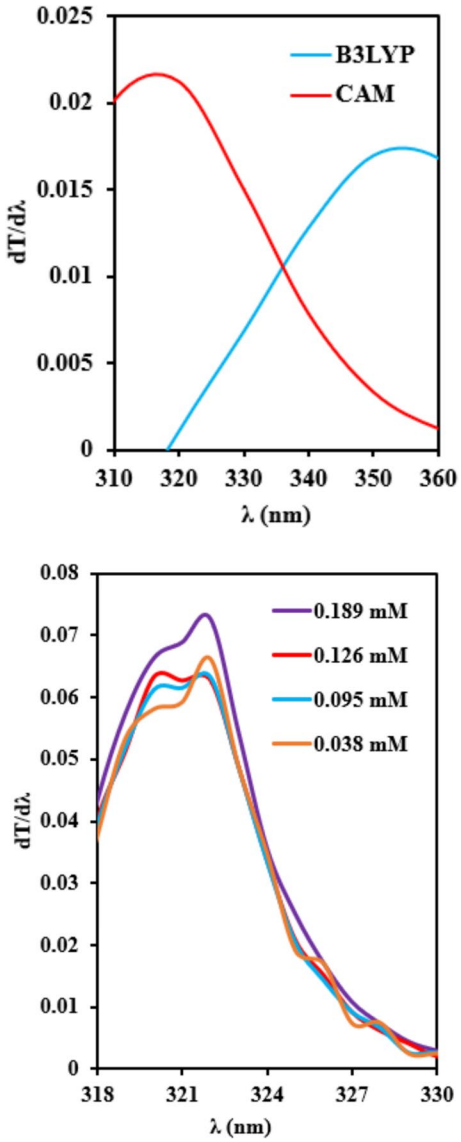

Fig. 5 The $dT/d\lambda$ plot vs. wavelength (λ) of BP-OXA organic material for DCM solvent

Table 1 The absorption band edge (E_{Abs-be}) and optical band gap (E_g) parameters of the BP-OXA

	E_g (eV)	E_{Abs-be} (eV)
B3LYP	3.375	3.482
CAM-B3LYP	3.807	3.910
EXP	3.844	3.855

value. A concentration value of 0.189 mM was used for this table and other optical parameters. BP-OXA material can be used in semiconductor technology according to E_{Abs-be} values. For this reason, we analyzed the optical band gap values of the molecule using the Tauc equation [56, 57],

$$(\alpha h\upsilon) = A\left(h\upsilon - E_g\right)^m \quad (1)$$

where $h\upsilon$ is the photon energy, A is a constant, and m is the parameter measuring the type of band gaps. While drawing Fig. 6, E and $(\alpha h\vartheta)^2$ curves were used. Here, E represents the photon energy, and $(\alpha h\vartheta)^2$ denotes direct transitions. Experimental and theoretical results from CAM-B3LYP and B3LYP are given in Table 1. Computational results show that the gap values of BP-OXA vary depending on the functional used. According to the table, optical band gaps and absorbance band edge values are compatible with each other. As can be seen from Table 1 and Fig. 6, the Eg and absorbance band edge values found with the CAM-B3LYP (3.81, 3.91 eV) functional yield better results compared to the experimental results (3.84, 3.86 eV). The Eg values obtained show that BP-OXA material exhibits semiconductor properties, indicating that this material can be used in optoelectronic applications.

Another parameter that should be considered in optical studies is the refractive index values [58, 59]. This value can be obtained from the spectrum plotted against the wavelength or with some equations depending on the optical band gap, such as

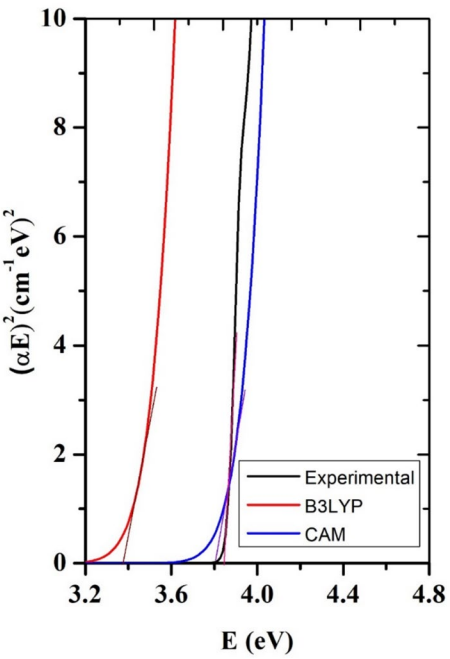

Fig. 6 The $(\alpha h\upsilon)^2$ vs photon energy (E) of BP-OXA

Kumar-Singh, Moss, Hervé-Vandamme, Ravindra, and Reddy. The refractive index values obtained from these equations are given experimentally and theoretically in Fig. 7. The refractive index values were found between 1.70 and 2.58 in the experimental, 1.72–2.58 in the CAM-B3LYP functional, and 1.98–2.67 in B3LYP with these equations. The high value of n is promising for optoelectronic uses. These values are in the range of semiconductor materials. As with the optical band gap (E_g) and absorbance band edge values, the values calculated with the CAM-B3LYP function are more compatible with the experimental data.

Optical conductivity $\left(\sigma_{\text{opt}}\right)$ and electrical conductivity $\left(\sigma_{\text{elct}}\right)$ are parameters that should be examined while investigating the optical properties of semiconductor materials. Optical conductivity is directly proportional to the absorption coefficient (α), refractive index (n), and speed of light (c), and electrical conductivity is inversely proportional to the absorption coefficient (α) and directly proportional to optical conductivity and wavelength (λ) [60]. If the absorption coefficient increases, the optical conductivity increases. The absorption coefficient is given by the following equation [22, 61].

$$\alpha = 2.303\frac{A}{d} \tag{2}$$

where A is the absorbance and d is the sample thickness. The spectrum of the absorption coefficient is similar to the absorption spectrum, as can be seen in the equation above (see Fig. 4). A high value of optical conductivity may indicate a highly excited electron state or high absorbance. This is a desired situation in the materials examined. Energy-dependent graphs of and parameters are experimental for CAM-B3LYP and B3LYP; Fig. 8a and b is given. Optical conductivity reached its maximum value at 4.07, 4.23, and 3.78 eV (experimental, CAM-B3LYP, and B3LYP), depending on absorbance. The second peak in the optical conductivity values is also very close (4.14, 4.56, 4.60). Similarly, the maximum value of electrical conductivity was found to be 3.95, 4.04, and 3.59 eV for the experimental CAM-B3LYP and B3LYP, respectively.

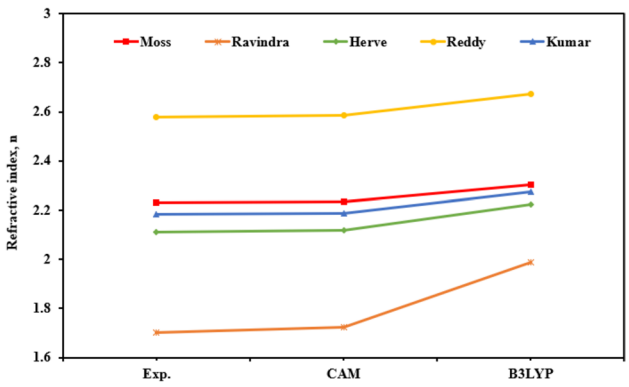

Fig. 7 The refractive index (n) curves wavelength (λ) of BP-OXA

3.5 Frontier molecular orbitals and density of states (DOS) analysis

A molecule's most important charge transfer transition is the transition from the highest occupied molecular orbital to the lowest unoccupied molecular orbital. With this transition, the energy gap value between the conductivity and valence bands can be found. This value is important for charge transfer [62, 63]. The transition between frontier molecular orbitals was calculated as 4.45 eV (B3LYP) and 6.47 eV (CAM-B3LYP) using the TD-DFT method. In the gas phase, this value is calculated as 4.45 eV. Experimentally, the Eg (optical band gap) value found in the DCM solvent is 3.844 eV. The Eg value calculated with the B3LYP and CAM-B3LYP functionals is 3.375 and 3.807 eV, respectively. According to these results, the B3LYP method provides better results in the transition between HOMO and LUMO in the BP-OXA molecule. Figure 9 is provided to illustrate the charge transfer in the molecule. According to Fig. 9, HOMO orbitals are localized throughout the molecule except for the oxygen and hydrogen atoms, while LUMO orbitals are localized throughout the molecule except for the hydrogen atoms.

Besides the interaction between HOMO and LUMO, it is important in transitions in neighboring orbitals [64]. To examine these transitions, orbital information and density of states between − 20 and 20 eV were investigated. The total density of state (TDOS or DOS) for BP-OXA was plotted with the GaussSum 2.2 program using the Gaussian output files found with the B3LYP and CAM-B3LYP functionals. Orbital information, density of state of the orbitals, and HOMO–LUMO charge transfer graphs are combined to form Fig. 9. The density in each orbital can be seen according to the DOS graph.

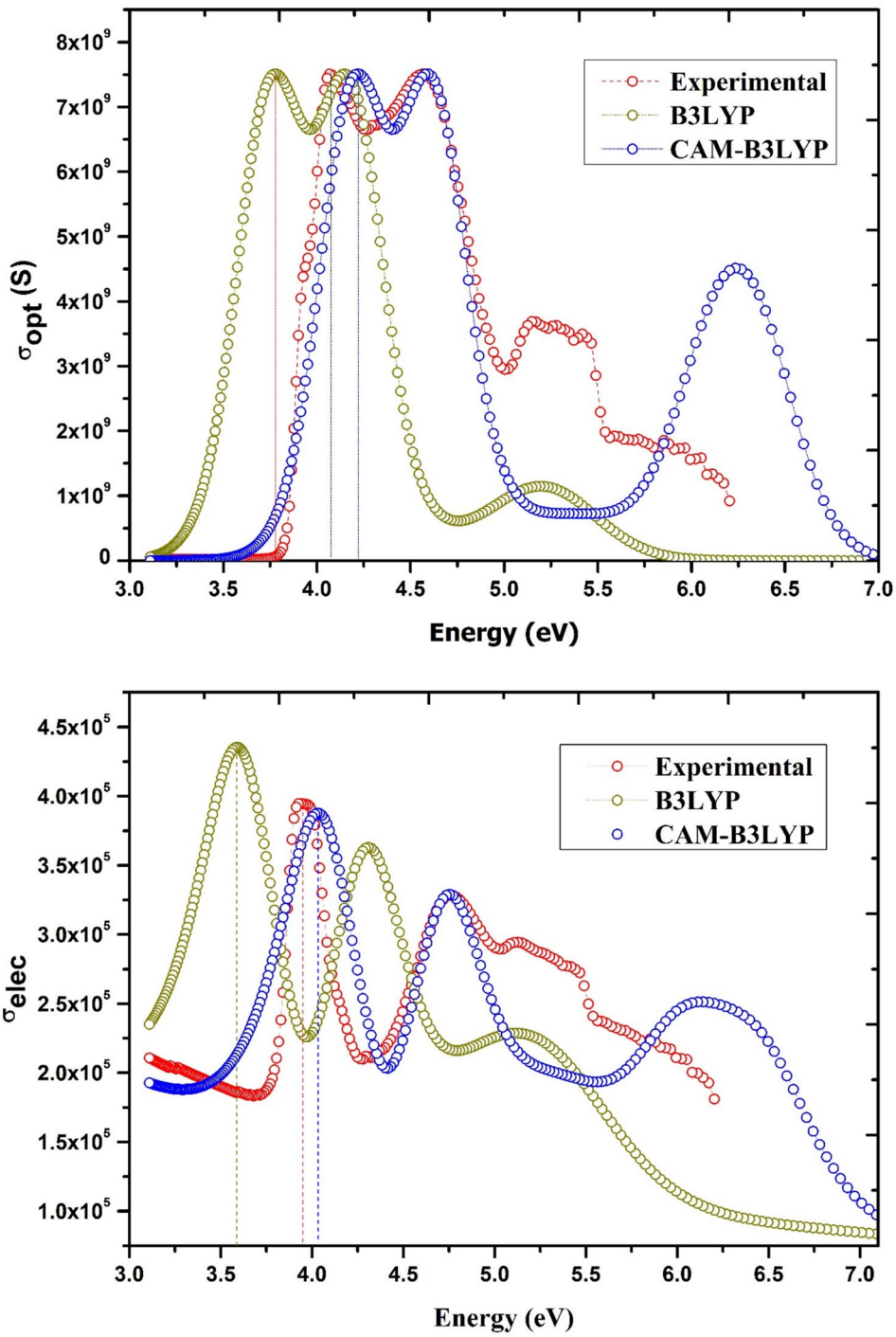

Fig. 8 a. The optical conductance (σ_{opt}) and b. electrical conductance (σ_{elect}) curves vs. (*E*) of BP-OXA

3.6 The atomic charges, dipole moments and NLO (non-linear optical) properties

The atomic charges of the BP-OXA molecule were determined by Mulliken population analysis and are given in Fig. 10. Atoms can have negative and positive atomic charges according to their positions in the molecule. All carbon atoms in the molecule except for C1 and C2 atoms in the oxadiazole ring has a negative charge. The oxygen atom in the oxadiazole ring has the lowest negative charge (− 0.29583e), and the carbon atom has the highest

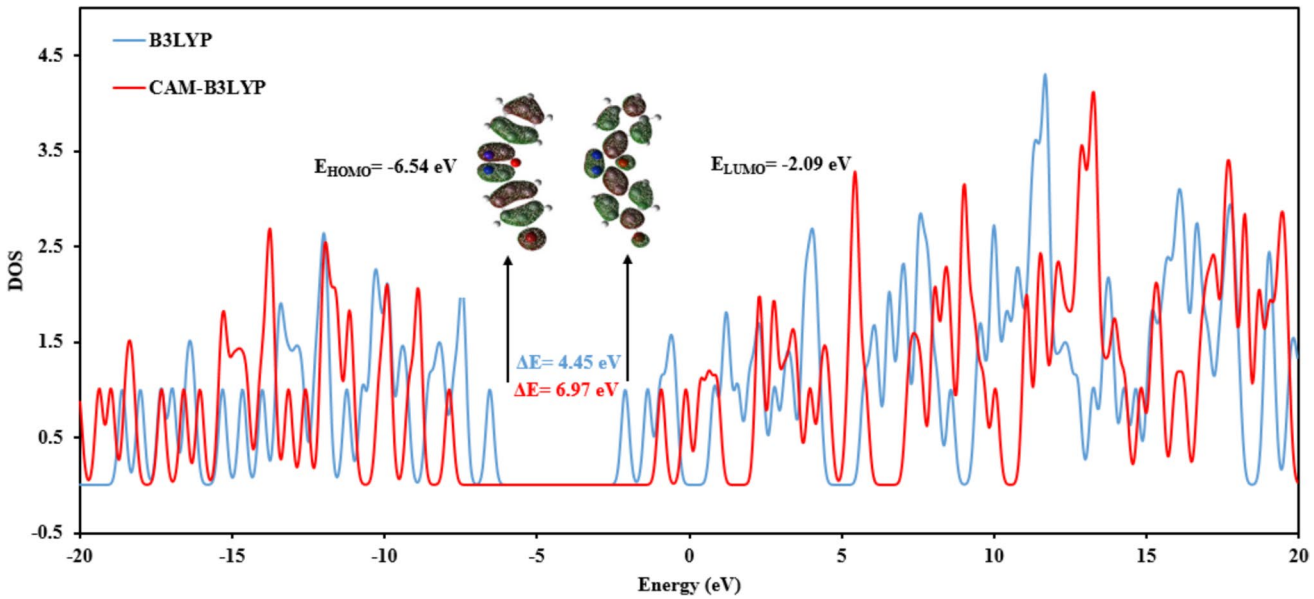

Fig. 9 Density of state (DOS) spectrum with HOMO–LUMO of BP-OXA

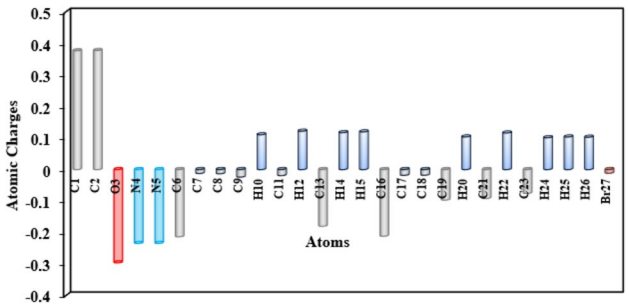

Fig. 10 Mulliken atomic charge of BP-OXA

positive charge (0.376896e). These values may be due to the O–C interaction in the oxadiazole ring. Since all hydrogen atoms in the BP-OXA molecule are acceptors, they have a positive charge and a charge of about 0.1e.

As can be seen from the Mulliken charge population, the BP-OXA molecule does not have a homogeneous charge distribution. The dipole moment resulting from the difference between negative and positive charges in the molecule is 3.3553 Debye in the gas phase. While the μ_y component contributes the greatest to the dipole moment, the μ_z component has no contribution. A high dipole moment value indicates a strong intermolecular interaction. The values in the DCM solvent are 4.3762 and 4.4279 Debye in the B3LYP and CAM-B3LYP functionalities, respectively. These values are tabulated in Table 2. Dipole moment values are compatible with the HOMO–LUMO energy gap, and large values mean that electrons can be excited easily.

Table 2 Dipole moment and its component for BP-OXA

	μ_x	μ_y	μ_z	μ_0
Vacuum	1.4887	− 3.007	0	3.3553
DCM (B3LYP)	1.6961	− 4.0342	0	4.3762
DCM (CAM-B3LYP)	1.7551	− 4.0652	0	4.4279

The quantum chemical parameters known as the nonlinear properties of the molecule were calculated with the following equations [59].

$$\langle \alpha \rangle = 1/3(\alpha xx + \alpha yy + \alpha zz)$$

$$\Delta\alpha = 1/2\left((\alpha xx - \alpha yy)^2 + (\alpha xx - \alpha zz)^2 + (\alpha yy - \alpha zz)^2\right)$$

$$\beta = \left[(\beta xxx + \beta xyy + \beta xzz)^2 + (\beta yyy + \beta yzz + \beta yxx)^2 + (\beta zzz + \beta zxx + \beta zyy)^2\right]$$

Table 3 The polarizability α (a.u.), the average polarizability α_o ($\times 10^{-24}$ esu), the anisotropy of the polarizability $\Delta\alpha$ ($\times 10^{-24}$ esu), and the first hyperpolarizability β ($\times 10^{-33}$ esu) of BP-OXA

α_{xx}	27.655087	β_{yyy}	− 4018.6995
α_{xy}	5.108127	β_{xxz}	0.0108
α_{yy}	52.338015	β_{xyz}	− 0.0061
α_{xz}	0.000122	β_{yyz}	0.2829
α_{yz}	− 0.002027	β_{xzz}	− 114.9666
α_{zz}	10.811993	β_{yzz}	− 91.1894
α_{total}	30.268365	β_{zzz}	0.0144
$\Delta\alpha$	60.02570337	β_x	− 2135.489392
β_{xxx}	− 845.0023	β_y	− 5072.316594
β_{xxy}	− 962.4277	β_z	0.308043745
β_{xyy}	− 1175.5205	β	5503.518027

The polarizability expressed by α is computed from the diagonal matrices of the quadrupole components, and the polarizability anisotropy expressed by $\Delta\alpha$ is computed from the diagonal and off-diagonal components of this matrix. First-order hyperpolarizability is represented by β and calculated using the above equation with data from the Gaussian output file. In the theoretical study of molecules, variables like polarizability and hyperpolarizability play a significant role in revealing details regarding nonlinear linear optical characteristics. Atomic units were changed to electronic units in order to acquire these values, which are shown in Table 3. It was discovered that the collected data was 100 times more polarized than urea, a polarized molecule (βtot = 5503.52 × 10^{-33} esu and $\Delta\alpha$ = 60.03 × 10^{-24} esu). These findings suggest that the BP-OXA molecule is a suitable NLO material. Fiber-optic telephony, optical switching, optical modulation, and optical data storage systems can all benefit from materials with higher hyperpolarizabilities than urea [64–66].

4 Conclusion

The electronic and optical properties of the organic material 2-(4-Bromophenyl)-5-phenyl-1,3,4-oxadiazole (BP-OXA) were extensively investigated using both experimental and theoretical approaches. This investigation was carried out using some spectroscopic techniques such as FT-IR and FT-Raman, ^{1}H and ^{13}C NMR, PL, and UV–Vis, and theoretical calculations. We found the molecule to have a C1 symmetry and a planar structure without any straining. In the FT-IR and FT-Raman spectra and the vibrational bands calculated by the DFT method, the most intense peak was observed to be the C=N stretching vibration, as expected. This band was assigned to the mixed C–C and C–N stretching vibration bands. ^{1}H and ^{13}C NMR chemical shift values of the BP-OXA molecule were found to be in the desired range and consistent with experimental data and similar molecules. Photoluminescence (PL) properties were evaluated by measurements performed at a 325 nm excitation wavelength, and the spectral band showed maximum emission around 733 nm. This band indicates a strong photoluminescence behavior with a red shift in the visible region. This indicates a structure with high quantum efficiency that suppresses the self-absorption of the BP-OXA molecule. The absorbance band edge of the molecule (~ 3.85 eV) and the optical band gap obtained by the Tauc method (~ 3.84 eV) confirm that BP-OXA has a wide band gap semiconductor character. Refractive index values (in the range of 1.70–2.58), high optical and electrical conductivity, HOMO–LUMO energy levels, and density of state (DOS) analyses revealed the efficiency of the molecule in terms of photon absorption and charge transfer mechanisms. In addition, high dipole moment and first-order hyperpolarizability value (β_tot = 5503.52 × 10^{-33} esu), which is approximately 100 times higher than urea, indicate that BP-OXA is promising for second-order nonlinear optical applications. Considering the research, the study of similar derivatives of the molecule can also be focused on.

Acknowledgements

This work was supported by Kirsehir Ahi Evran University Scientific Project Unit (BAP), Project No: TBY. A4.19.001.

Funding

Open access funding provided by the Scientific and Technological Research Council of Türkiye (TÜBİTAK). The authors declare that no funds, grants, or other support were received during the preparation of this manuscript.

Data availability

Data sets generated during the current study are available from the corresponding author on reasonable request.

Declarations

Competing interests The authors have no relevant financial or non-financial interests to disclose.

Research involving human and animal rights The authors declare that there are no potential conflicts of interest associated with this study. Furthermore, the research did not involve any experiments on human participants or animals. As no human subjects were involved, the requirement for informed consent was not applicable.

References

1. M.S. Najare, M.K. Patil, A.A. Nadaf, S. Mantur, S.R. Inamdar, I.A.M. Imtiyaz, Synthesis, characterization and photophysical properties of a new class of pyrene substituted 1,3,4-oxadiazole derivatives. Opt. Mater. **88**, 256–265 (2019)
2. A.K. Maniyar, Y.F. Nadaf, S. Khasim et al., Photophysical studies on donor-p-acceptor substituted 1,3,4-oxadiazole derivatives for optoelectronic application: experimental and theoretical analysis. J. Opt. **3**, 1–2 (2024)
3. M.S. Najare, M.K. Patil, T.S. Tilakraj et al., Photophysical and electrochemical properties of highly π-conjugated bipolar carbazole-1,3,4-oxadiazole-based D–π–A type of efficient deep blue fluorescent dye. J. Fluoresc. **31**, 1645–1664 (2021)
4. B. Waddar, S. Gandi, S.R. Parne, V.R. Chari, G.R. Prasanth, Investigation of second-order NLO properties of novel 1,3,4-oxadiazole derivatives: a DFT study. J. Mol. Model. **30**(5), 118 (2024)
5. A.-R. Lee, J. Lee, J. Lee, W.-S. Han, Silicon-based carbazole and oxadiazole hybrid as a bipolar host material for phosphorescent organic light-emitting diodes. Org. Electron. **38**, 222–229 (2016)
6. J.A. Mikroyannidis, L. Fenenko, C. Adachi, Synthesis and photophysical characteristics of 2,7-fluorenevinylene-based trimers and their electroluminescence. J. Phys. Chem. B **110**, 20317–20326 (2006)
7. F. Chen, T. Tian, C. Zhao, B. Bai, M. Li, H. Wang, Substituent effect on photophysical properties of bi-1,3,4-oxadiazole derivatives in solution. J. Mol. Struct. **1109**, 239–246 (2016)
8. C.I.L. Alongamo, S.N. Tasheh, N.K. Nkungli, F.K. Bine, J.N. Ghogomu Structural, electronic, and charge transport properties of new materials based on 2-(5-Mercapto-1, 3, 4-Oxadiazol-2-yl) phenol for organic solar cells and light emitting diodes by DFT and TD-DFT. J. Chem. **2022**(1), 1802826 (2022)
9. H. Ye, H. Wu, L. Chen, S. Ma, K. Zhou, G. Yan, J. Shen, D. Chen, S.J. Su, Synthesis, properties, calculations and applications of small molecular host materials containing oxadiazole units with different nitrogen and oxygen atom orientations for solution-processable blue phosphorescent OLEDs. Electron. Mater. Lett. **14**, 89–100 (2018).
10. X. Zhao, Y. Li, F. Chen, H. Wang, M. Li, H. Wang, Y. Shi, Intramolecular charge transfer dynamics in the excited states of diphenylamine substituted 1, 3, 4-oxadiazole derivatives. Spectrochim. Acta Part A **267**, 120463 (2022)
11. Y.T. Chang, J.K. Chang, Y.T. Lee, P.S. Wang, J.L. Wu, C.C. Hsu, C.I. Wu, High-efficiency small-molecule base-dorganic light emitting devices with solution processes and oxadiazole-based electron transport materials. ACS Appl. Mater. Interfaces. **5**(21), 10614–10622 (2013)
12. J. Pommerehne, H. Vestweber, W. Guss, R.F. Mahrt, H. Bässler, M. Porsch, Efficient two layer leds on apolymer blend basis. J. Daub Av. Anne. **7**, 551 (1995)

13. A. Paun, N.D. Hadade, C.C. Paraschivescu, M. Matache, 1,3,4-Oxadiazoles as luminescent materials for organic light emitting diodes via cross-coupling reactions. J. Mater. Chem. C (2016). https://doi.org/10.1039/C6TC03003C
14. B. Schultz, M. Bruma, L. Brehmer, Aromatic poly (1, 3, 4-oxadiazoe)s as advanced materials. AdV. Mater. **9**, 601 (1997)
15. M. Thelakkat, H.-W. Schmidt, Low molecular weight and polymeric heterocyclics as electron transport/hole-blocking materials in organic light-emitting diodes. Polym. Adv. Technol. **9**, 429 (1998)
16. K. Chondroudis, D.B. Mitzi, Electroluminescence from an organic−inorganic perovskite incorporating aquaterthiophene dye within lead halide perovskite layers. Chem. Mater. **11**, 3028 (1999)
17. C. Wang, G.-Y. Jung, A.S. Batsanov, M.R. Bryce, M.C. Petty, New electron-transporting materials for light emitting diodes: 1, 3, 4-oxadiazole–pyridine and 1, 3, 4-oxadiazole–pyrimidine hybrids. J. Mater. Chem. **12**, 173 (2002)
18. S.W. Cha, S.-H. Choi, K. Kim, K.J.-I. Jin, Synthesis and luminescence properties of four-armed conjugated structures containing 1, 3, 4-oxadiazole moieties. J. Mater. Chem. **13**, 1900 (2003)
19. A.P. Kulkarni, C.J. Tonzola, A. Babel, S.A. Jenekhe, Electron transport materials for organic light-emitting diodes. Chem. Mater. **16**, 4556 (2004)
20. D.-H. He, X.-W. Li, C. Yang, J. Yang, Characterization and optical properties of novel unsymmetrical stilbene-based 1,3,4-oxadiazole derivatives. Spectrochim. Acta Part A **95**, 184–187 (2012)
21. S. Nayak, R.K. Sinha, P.M. Lewis, S.D. Kulkarni, S.L. Gaonkar, Synthesis, characterization, DFT and photophysical studies of new class of 1, 3, 4-oxadiazole-isobenzofuran hybrids. J. Lumin. **238**, 118212 (2021)
22. E.B. Sas, M. Kurban, B. Gündüz, M. Kurt, Photophysical, spectroscopic properties and electronic structure of BND: experiment and theory. Synth. Met. **246**, 39–44 (2018)
23. Q. Wu, R. Braveenth, H.Q. Zhang, I.-J. Bae, M. Kim, K.Y. Chai, Oxadiazole-based highly efficient bipolar fluorescent emitters for organic light-emitting diodes. Molecules **23**(4), 843 (2018)
24. S.S. Reddy, V.G. Sree, W. Cho, S.-H. Jin, Achieving pure deep-blue electroluminescence with CIE $y \leq 0.06$ via a rational design approach for highly efficient non-doped solution-processed organic light-emitting diodes. Chem. Asian J. **11**, 3275–3282 (2016)
25. S.-J. Woo, Y. Kim, M.-J. Kim, J.Y. Baek, S.K. Kwon, Y.H. Kim, J.J. Kim, Strategies for the molecular design of donor–acceptor-type fluorescent emitters for efficient deep blue organic light emitting diodes. Chem. Mater. **30**, 857–863 (2018)
26. S.S. Reddy, V.G. Sree, K. Gunasekar, W. Cho, Y.S. Gal, M. Song, J.W. Kang, S.H. Jin, Highly efficient bipolar deep-blue fluorescent emitters for solution-processed non-doped organic light-emitting diodes based on 9,9-dimethyl-9,10-dihydroacridine/phenanthroimadazole derivatives. Adv. Opt. Mater. **4**, 1236–1246 (2016)
27. D. Thirion, J. Rault-Berthelot, L. Vignau, C. Poriel, Synthesis and properties of a blue bipolar indenofluorene emitter based on a D–π–A design. Org. Lett. **13**, 4418–4421 (2011)
28. T. Zhang, S. Jiang, G. Wang, Y. Zuo, S. Yu, Q. Zhang, X. Hu, 1, 3, 4-Oxadiazole derivative: photophysical, gelation, self-assembly, and Fe^{3+} fluorescence sensing properties. J. Chem. Res. **48**(3), 17475198241255788 (2024)
29. P. Hohenberg, W. Kohn, Density functional theory (DFT). Phys. Rev. **136**, B864–B871 (1964)
30. W. Kohn, L.J. Sham, Self-consistent equations including exchange and correlation effects. Phys. Rev. **140**, A1133 (1965)
31. Internet References, https://cccbdb.nist.gov/vibscalejustx.asp (2025)
32. K. Wolinski, J.F. Hinton, P. Pulay, Efficient implementation of the gauge-independent atomic orbital method for NMRchemical shift calculations. J. Am. Chem. Soc. **112**, 8251–8260 (1990)
33. A.D. Becke, Density-functional thermochemistry. III. The role of exact exchange. J. Chem. Phys. **98**, 5648–5652 (1993)
34. T. Yanai, D.P. Tew, N.C. Handy, A new hybrid exchange–correlation functional using the Coulomb-attenuating method (CAM-B3LYP). Chem. Phys. Lett. **393**, 51 (2004)
35. M.J. Frisch, G.W. Trucks, H.B. Schlegel, G.E. Scuseria, M.A. Robb, J.R. Cheeseman, J.B. Cross, *Gaussian 09, Revision A*, 1st edn. (Gaussian. Inc., Wallingford, 2009)
36. N.M. O'Boyle, A.L. Tenderholt, K.M. Langner, Cclib: a library for package-independent computational chemistry algorithms. J. Comput. Chem. **29**, 839–845 (2008)
37. M. Silverstein, G. ClaytonBasseler, C. Morill, *Spectrometric Identification of Organic Compounds* (Wiley, New York, 2001)
38. J.S. Murray, K. Sen, *Molecular Electrostatic Potentials, Concepts and 399 Applications* (Elsevier, Amsterdam, 1996)
39. G. Varsanyi, *Assignments of Vibrational Spectra of Seven Hundred Benzene Derivatives* (Adam Hilger, London, 1974)
40. M. Karabacak, E. Kose, A. Atac, E.B. Sas, A.M. Asiri, M. Kurt, Experimental (FT-IR, FT-Raman, UV–Vis, 1H and

13C NMR) and computational (density functional theory) studies on 3-bromophenylboronic acid. J. Mol. Struct. **1076**, 358–372 (2014)
41. E.B. Sas, E. Kose, M. Kurt, M. Karabacak, FT-IR, FT-Raman, NMR and UV–Vis spectra and DFT calculations of 5-bromo-2-ethoxyphenylboronic acid (monomer and dimer structures). Spectrochim. Acta Part A **137**, 1315–1333 (2015)
42. T. Schlick, *Molecular Modeling and Simulation: An Interdisciplinary Guide*, 2nd edn. (Springer, New York, 2010)
43. H.O. Kalinowski, S. Berger, S. Braun, *Carbon-13 NMR Spectroscopy* (Wiley, Chichester, 1988)
44. K. Pihlaja, E. Kleinpeter (eds.), *Carbon-13 Chemical Shifts in Structural and Sterochemical Analysis* (VCH Publishers, Deerfield Beach, 1994)
45. N. Subramania, N. Sundaraganesan, J. Jayabharathi, Molecular structure, spectroscopic (FT-IR, FT-Raman, NMR, UV) studies and first-order molecular hyperpolarizabilities of 1, 2-bis (3-methoxy-4-hydroxybenzylidene) hydrazine by density functional method. Spectrochim. Acta A **76**, 259–269 (2010)
46. E.B. Sas, M. Kurt, M. Can, N. Horzum, A. Atac, Spectroscopic studies on 9H-carbazole-9-(4-phenyl) boronic acid pinacol ester by DFT method. J. Mol. Struct. **1118**, 124–138 (2016)
47. H.B. Bebb, E.W. Williams, Photoluminescence I: theory, in *Semiconductors and Semimetals*. ed. by H.B. Bebb, E.W. Williams (Elsevier, Amsterdam, 1972), pp.181–320
48. V.K. Evgeny, V.T. Nikita, L. MikhailYu, G.M. Vladimir, V.B. Alexander, V.F. Anatoly, D.R. Ivan, L.R. Andrey, Aminofunctionalization of carbon dots leads to red emission enhancement. J. Phys. Chem. Lett. **10**, 5111–5116 (2019)
49. S. Li, K. Dong, M. Cai, X. Li, X. Chen, A plasmonic S-scheme Au/MIL-101 (Fe)/BiOBr photocatalyst for efficientsynchronous decontamination of Cr (VI) and norfloxacin antibiotic. eScience **4**(2), 100208 (2024)
50. S. Li, M. Cai, Y. Liu, C. Wang, R. Yan, X. Chen, Constructing $Cd_{0.5}Zn_{0.5}S/Bi_2WO_6$ S-scheme heterojunction forboosted photocatalytic antibiotic oxidation and Cr(VI) reduction. Adv. Powder Mater. **2**(1), 100073 (2023)
51. H.M. Albert, T. Jemima, C.A. Gonsago, Synthesis, spectroscopic, optical, and thermal characterizations of zinc (tris)-thiourea sulfate: a metal–organic crystal. J. Fluoresc. **34**(3), 1057–1063 (2024)
52. H.M. Albert, P. Padmavathi, A. Mahalakshmi, G.V.S. Srinivas, M.K. Chakravarthi, M.R. Babu, C.A. Gonsago et al., Exploring the spectroscopic, photoluminescence, thermal, dielectric, and electrical conductivity properties of 4-aminopyridine nitrate (4APN): a semi-organic material. J. Mater. Res. **40**, 1–11 (2025)
53. C. Bettinali, V. Gottardi, B. Locardi, Luminescence and structure in lead silicate glasses. J. Non-Cryst. Solids **1**, 360–370 (1969)
54. S.A. Abdel-Hameed, F.H. Margha, Influence of PbO content on the glass forming ability, crystallization, electrical, UV–Vis and photoluminescence spectroscopy properties of LiF. PbO system. Ceram. Int. **50**(2), 3584–3595 (2024)
55. R. Zhou, X. Lu, Q. Yang, P. Wu, Chin. Nanocrystals for large Stokes shift-based optosensing. Chem. Lett. **30**, 1843–1848 (2019)
56. J. Tauc, A. Menth, States in the gap. J. Non-Cryst, Solids **569**, 8 (1972)
57. E.B. Sas, Characterization, optical and nonlinear optical properties of TAZ organic material. Optik **188**, 91–98 (2019)
58. B. Gündüz, Optical properties of poly[2-methoxy-5-(3′,7′-dimethyloctyloxy)-1,4-phenylenevinylene] light-emitting polymer solutions: effects of molarities and solvents. Polym. Bull. **72**(12), 3241–3267 (2015)
59. E.B. Sas, E. Tanış, B. Gündüz, M. Kurt, Comparison of theoretical and experimental electronic and optoelectronic properties of HPS compound. Mater. Res. Express **6**(12), 126210 (2020)
60. M. Yarmohammadi, Strain effects on the optical conductivity of gapped graphene in the presence of Holstein phonons beyond the Dirac cone approximation. AIP Adv. **6**, 085008 (2016)
61. G. Soni, S. Srivastava, P. Soni, P. Kalotra, Y.K. Vijay, Optical, mechanical and structural properties of PMMA/SiO_2 nanocomposite thin films. Mater. Res. Express **5**, 015302 (2001)
62. K. Fukui, Role of frontier orbitals in chemical reactions. Science **218**, 747–754 (1982)
63. M. Arivazhagan, D. Anitha, Rexalin. Spectrochim. Acta A **96**, 668–676 (2012)
64. R. Hoffmann, *Solids and Surfaces: A Chemist's View of Bonding in Extended Structures* (VCH Publishers, New York, 1988)
65. Z. Feng, J. Wang, Y. Wang, C. Ye, Study on nonlinear optical active NPP and PNP acrylate copolymers. Synth. Met. **57**, 3945–3950 (1993)
66. T.S.M. KariduraganavarMY, R.G. Tasaganva, A.A. Kittur, S.S. Kulkarni, S.R. Inamdar, Studies on nonlinear optical polyurethanes containing heterocyclic chromophores. J. Mol. Struct. **987**, 158–165 (2011)